

Inflammasome activation in COVID-19 patients

Tamara S. Rodrigues¹, Keyla S.G. de Sá¹, Adriene Y. Ishimoto¹, Amanda Becerra¹, Samuel Oliveira¹, Leticia Almeida^{1,2}, Augusto V. Gonçalves¹, Debora B. Perucello¹, Warrison A. Andrade¹, Ricardo Castro³ Flavio P. Veras⁴, Juliana E. Toller-Kawahisa⁴, Daniele C. Nascimento⁴, Mikhael H.F. de Lima⁴, Camila M. S. Silva⁴, Diego B. Caetite⁴, Ronaldo B. Martins¹, Italo A. Castro¹, Marjorie C. Pontelli¹, Fabio C. de Barros^{5,6}, Natália B. do Amaral⁷, Marcela C. Giannini⁷, Letícia P. Bonjorno⁷, Maria Isabel F. Lopes⁷, Maíra N. Benatti⁷, Rodrigo C. Santana⁷, Fernando C. Vilar⁷, Maria Auxiliadora-Martins⁸, Rodrigo Luppino-Assad⁷, Sergio C.L. de Almeida⁷, Fabiola R. de Oliveira⁷, Sabrina S. Batah⁹, Li Siyuan⁹, Maira N. Benatti⁹, Thiago M. Cunha^{2,4}, José C. Alves-Filho^{2,4}, Fernando Q. Cunha^{2,4}, Larissa D. Cunha¹, Fabiani G. Frantz³, Tiana Kohlsdorf⁵, Alexandre T. Fabro⁹, Eurico Arruda¹, Renê D.R. de Oliveira⁷, Paulo Louzada-Junior⁷, Dario S. Zamboni^{1,2*}

¹Departamento de Biologia Celular e Molecular e Bioagentes Patogênicos and ²Center of Research in Inflammatory Diseases (CRID), Faculdade de Medicina de Ribeirão Preto, Universidade de São Paulo, Ribeirão Preto, São Paulo, Brazil.

³Departamento de Análises Clínicas, Toxicológicas e Bromatologia, Faculdade de Ciências Farmacêuticas de Ribeirão Preto, Universidade de São Paulo, Ribeirão Preto, SP, Brazil.

⁴Departamento de Farmacologia, Faculdade de Medicina de Ribeirão Preto, Universidade de São Paulo, Ribeirão Preto, São Paulo, Brazil.

⁵Departamento de Biologia, Faculdade de Filosofia Ciências e Letras de Ribeirão Preto, Universidade de São Paulo, Ribeirão Preto, SP, Brazil.

⁶Departamento de Ecologia e Biologia Evolutiva, Instituto de Ciências Ambientais, Químicas e Farmacêuticas, Universidade Federal de São Paulo, Diadema, SP, Brazil.

⁷Divisão de Imunologia Clínica, Emergência, Doenças Infecciosas e Unidade de Terapia Intensiva, Faculdade de Medicina de Ribeirão Preto, Universidade de São Paulo, Ribeirão Preto, SP, Brazil.

⁸Divisão de Medicina Intensiva, Departamento de Cirurgia e Anatomia, Faculdade de Medicina de Ribeirão Preto, Universidade de São Paulo, Ribeirão Preto, SP, Brazil.

⁹Departamento de Patologia e Medicina Legal, Faculdade de Medicina de Ribeirão Preto, Universidade de São Paulo, Ribeirão Preto, SP, Brazil.

*Correspondence:

Dario S. Zamboni, Ph.D.

Departamento de Biologia Celular e Molecular e Bioagentes Patogênicos. Av. Bandeirantes 3900, Ribeirão Preto, SP 14049-900 Brazil.

Tel: (55) (16) 3602-3265.

Fax: (55) (16) 3633-1786.

E-mail: dszamboni@fmrp.usp.br

47 **Abstract**

48

49 Severe cases of COVID-19 are characterized by a strong inflammatory
50 process that may ultimately lead to organ failure and patient death. The NLRP3
51 inflammasome is a molecular platform that promotes inflammation via cleavage and
52 activation of key inflammatory molecules including active caspase-1 (Casp1p20), IL-
53 1 β and IL-18. Although the participation of the inflammasome in COVID-19 has been
54 highly speculated, the inflammasome activation and participation in the outcome of
55 the disease is unknown. Here we demonstrate that the NLRP3 inflammasome is
56 activated in response to SARS-CoV-2 infection and it is active in COVID-19,
57 influencing the clinical outcome of the disease. Studying moderate and severe
58 COVID-19 patients, we found active NLRP3 inflammasome in PBMCs and tissues of
59 post-mortem patients upon autopsy. Inflammasome-derived products such as
60 Casp1p20 and IL-18 in the sera correlated with the markers of COVID-19 severity,
61 including IL-6 and LDH. Moreover, higher levels of IL-18 and Casp1p20 are
62 associated with disease severity and poor clinical outcome. Our results suggest that
63 the inflammasome is key in the pathophysiology of the disease, indicating this
64 platform as a marker of disease severity and a potential therapeutic target for COVID-
65 19.

66

67

68 COVID-19 is an inflammatory disease caused by the severe acute respiratory
69 syndrome coronavirus 2 (SARS-CoV-2), which can manifest a broad spectrum of
70 symptoms ranging from little or no symptoms to severe pneumonia that may evolve to
71 acute respiratory distress syndrome (ARDS) and death ¹. While the molecular
72 mechanisms driving disease severity are still unclear, the clinical association of
73 inflammatory mediators such as IL-6 and lactate dehydrogenase (LDH) with severe
74 cases suggests that excessive inflammation is central for the poor clinical outcome ²⁻⁵.
75 The induction of inflammatory processes in the host cell often requires the
76 engagement of the inflammasomes, which are protein platforms that aggregate in the
77 cytosol in response to different stimuli ⁶. The NLRP3 inflammasome, possibly the
78 most studied one of such platforms, comprises the NLRP3 receptor, the adaptor
79 molecule ASC, and caspase-1. Caspase-1 is activated by proteolytically cleavage and
80 promotes the activation of many substrates, including the inflammatory cytokines IL-
81 1 β and IL-18 and Gasdermin-D, a pore-forming protein that induces an inflammatory
82 form of cell death called pyroptosis ⁶. NLRP3 activation in response to microbial
83 infections, cell damage, or aggregates in the host cell cytoplasm promotes ASC
84 polymerization, leading to the formation of a micron-sized structure called puncta (or
85 speck) that is a hallmark of active inflammasomes in the cells ⁷.

86

87 The pronounced inflammatory characteristics of COVID-19 and the
88 correlation of disease severity with the pyroptosis marker LDH prompted us to
89 investigate the activation of the inflammasome by SARS-CoV-2 and its role in
90 disease development. Initially, we infected primary human monocytes in vitro with
91 SARS-CoV-2 and assessed inflammasome activation. Using monocytes from

92 different healthy donors, we found that SARS-CoV-2 infection triggers LDH release
93 and activation of NLRP3 inflammasome in monocytes, as shown by NLRP3 puncta
94 formation (**Fig. 1A-C**). As expected, uninfected cells were negative for dsRNA
95 staining and NLRP3 puncta formation. Nigericin, a bacterial toxin known to trigger
96 NLRP3 inflammasome, was used as a positive control. Activation of the NLRP3
97 inflammasome required viable virus particles, as UV-inactivated SARS-CoV-2 failed
98 to induce NLRP3 puncta formation (**Fig. 1B**). We also measured the activation of IL-
99 1β as a readout for inflammasome activation and found that infection with SARS-
100 CoV-2 caused the production of IL- 1β in primed cells, as measured by ELISA (**Fig.**
101 **1D**). We measured the viral load using RT-PCR and confirmed that SARS-CoV-2
102 infects and replicates in primary human monocytes in vitro (**Fig. 1E**). We also tested
103 infection in primary human monocyte-derived macrophages and found that SARS-
104 CoV-2 infection triggers macrophage cell death in a dose-dependent effect as shown
105 by the presence of LDH in the supernatants (**Fig. 1F**). Nigericin was used as positive
106 control and UV-inactivated virus as a negative control. We next tested the
107 inflammasome activation in the sera of COVID-19 patients. It was previously shown
108 that IL- 1β is activated independently of caspase-1 in vivo⁸⁻¹⁰, thus we assessed
109 active/cleaved caspase-1 (Casp1p20) and cleaved IL-18 as readouts for
110 inflammasome activation in COVID-19 patients. We tested sera from 124 COVID-19
111 patients obtained on the day of hospitalization (all tested RT-PCR positive for SARS-
112 CoV-2) and compared with sera of 42 controls that tested RT-PCR/serology negative
113 or that were collected before the COVID-19 pandemic. We found higher
114 concentrations of Casp1p20 and IL-18 in the sera of patients (**Fig. 2A, B**), suggesting
115 active inflammasome in COVID-19 patients. We also found that IL-6, IL-10, IL-4
116 were increased in patients as compared to controls, whereas we do not detect

117 statistically significant differences for IL-2, TNF- α , and IL-17A (**Fig. 2C and Fig.**
118 **S1**). IFN- γ levels were slightly lower in COVID-19 patients as compared to controls
119 (**Fig. S1**). Next, we measured inflammasome activation in peripheral blood
120 mononuclear monocytes (PBMCs) from 47 patients and compared them with 32
121 healthy individuals. Using the FAM-YVAD assay that stains active intracellular
122 caspase-1¹¹, we found that, on the day of hospitalization, the PBMCs from patients
123 show a higher percentage of FAM-YVAD⁺ cells as compared to healthy controls
124 (**Fig. 2D-E**). Microscopy observation of these cells allows clear visualization of
125 NLRP3 puncta in PBMCs, indicating active inflammasomes in patients cells (**Fig. 2F-**
126 **G**). We further confirmed caspase-1 activation using a luminescent assay and found
127 active caspase-1 in supernatants from 46 patients PBMCs cultures, as opposed to low
128 caspase-1 activation in healthy donors (**Fig. 2H**). We also detected IL-1 β in the
129 supernatants of PBMCs from some patients, but not from healthy donors (**Fig. 2I**),
130 further supporting inflammasome activation in PBMCs from COVID-19 patients.

131

132 We further assessed inflammasome activation in lung tissues obtained from
133 autopsies of deceased COVID-19 patients. Using an anti-SARS-CoV-2 antibody, we
134 first confirmed viral presence by immunohistochemical staining SARS-CoV-2 in
135 injured regions of post-mortem lung tissues (**Fig. 3A,B**). We then performed
136 Multiplex Staining by Sequential Immunohistochemistry with SARS-CoV-2, anti-
137 CD14, and anti-NLRP3 and identified infected CD14⁺ cells expressing NLRP3 in
138 post-mortem tissues (**Fig. 3C, D**). Using multiphoton microscopy, we quantified the
139 number of NLRP3 puncta in tissues 5 controls and 6 COVID-19 patients and found
140 that patients contain higher numbers of NLRP3 puncta as compared to controls. (**Fig.**
141 **3E**). Images of tissues stained with anti-NLRP3 antibody illustrates NLRP3 puncta in

142 of lethal cases of COVID-19 (**Fig. 3F-I**). We observed NLRP3 puncta inside cells in
143 the tissues and also cells contained in venules (**Fig. 3I**), unequivocally demonstrating
144 activation of the NLRP3 inflammasome in fatal cases of COVID-19.

145

146 We next assessed the impact of the inflammasome activation in the clinical
147 outcome of the disease. Initially, we performed analyses using the levels of Casp1p20
148 and IL-18 in 124 patients sera obtained on the day of hospitalization. A correlation
149 matrix show association of Casp1p20 and IL-18 levels with patient characteristics and
150 clinical parameters (**Fig. 4A**). As expected, we found a positive correlation between
151 Casp1p20 and IL-18 levels (**Fig. 4B**). In addition, Casp1p20 positively correlated
152 with IL-6, LDH and C-reactive protein (CRP) (**Fig. 4C-E**). Furthermore, we found
153 that IL-18 levels positively correlated with IL-6 and CRP levels (**Fig. 4F, G**). We also
154 evaluated if the levels of Casp1p20 and IL-18 were affected by patients comorbidities
155 and clinical parameters, including bacterial co-infections (cultivable bacteria in the
156 blood), nephropathy, obesity, gender, cerebrovascular accident, pneumopathy,
157 immunodeficiency and neoplasia (**Fig. S2**). We only detected statistically significant
158 differences when we compared obese with non-obese patients, as the levels of IL-18
159 were higher in patients with body mass index ≥ 30 (**Fig. S2G**).

160

161 Next, we investigated if Casp1p20 and IL-18 levels measured on the day of
162 hospitalization correlated with the clinical outcome of the disease. Importantly, we
163 found that IL-18, but not Casp1p20 were higher in patients who required mechanical
164 ventilation (MV) as compared with patients that did not (**Fig. 4H, I**). When we
165 separated the patients according to the severity of the disease (mild/moderate versus
166 severe), we found that the levels of Casp1p20 but not IL-18 were higher in patients

167 with the severe form of COVID-19 (**Fig. 4J, K**). We also observed that the levels of
168 IL-18, but not Casp1p20, were higher in lethal cases of COVID-19 as compared to
169 survivors (**Fig. 4L, M**). Finally, we performed longitudinal analyses of IL-18 and
170 Casp1p20 production in 37 patients from the day of hospitalization (day zero) for up
171 to 45 days post-admission using generalized mixed models with ‘gamma’ distribution
172 and ‘log’ link function as the best dataset prediction. For these analyses, we
173 categorized the patients as Death, Mild-Recovery (patients that were hospitalized but
174 did not require mechanical ventilation and recovered), and Critical-Recovery (patients
175 that required mechanical ventilation at the Intensive Care Unit (ICU) and recovered)
176 (**Supplemental data**). For Casp1p20, the most parsimonious model indicated a
177 significant effect of the day sampled, and the production level decreased with time
178 regardless of sex or patient outcome (**Fig. 4N**, and **Supplemental data**). For IL-18,
179 the best-fit model retained also described an overall reduction in IL-18 production
180 along time (Day sampled), which differed among patient groups. This model
181 predicted a decrease in IL-18 at similar rates among the three groups, with patients
182 that died presenting higher levels (intercept) that never reached those observed in
183 mild and critical recovered patients (**Fig. 4O** and **Supplemental data**), supporting our
184 assertion that the magnitude of inflammasome activation impacts the disease
185 outcome. In summary, our data demonstrate that the inflammasome is robustly active
186 in COVID-19 patients requiring hospitalization. It also supports that both the
187 magnitude of inflammasome activation at the hospitalization day and the course of
188 inflammasome activation during hospitalization influenced the clinical outcome.
189 Collectively, our observations suggest that the inflammasome is key for the induction
190 of the massive inflammation observed in severe and fatal cases of COVID-19. Our

191 study supports the use of inflammasome activation both as a marker of disease
192 severity and prognostic but also as a potential therapeutic target for COVID-19.

193

194

195 **Materials and methods**

196

197 **Patients**

198 A total of 124 patients with COVID-19 that were tested positive using RT-PCR as
199 described previously ^{12,13}. Patients were classified according to their clinical
200 manifestations in: i) mild cases: the clinical symptoms are mild and no pneumonia
201 manifestations can be found in imaging; ii) moderate cases: patients have symptoms
202 such as fever and respiratory tract symptoms, etc. and pneumonia manifestations can
203 be seen in imaging; iii) severe cases: adults who meet any of the following criteria:
204 respiratory rate ≥ 30 breaths/min; oxygen saturations; 93% at a rest state; arterial
205 partial pressure of oxygen (PaO₂)/oxygen concentration (FiO₂) < 300 mm Hg ¹⁴.
206 Patients were enrolled in HC-FMRP/USP from April 06 to July 02, 2020 and **Table**
207 **S1** summarizes clinical, laboratory, and treatment records. We also collected samples
208 from 73 age and gender-matched healthy controls. Controls were collected either
209 before the COVID-19 pandemic or tested negative for COVID-19 using RT-PCR
210 and/or serology (specific IgM and IgG antibodies) (Asan Easy Test.COVID-19
211 IgM/IgG kits, Asan Pharmaceutical Co.).

212

213 **Peripheral blood mononuclear cells isolation**

214 Whole blood was collected from healthy donors (Ethics Committee Protocol from the
215 Clinical Hospital of Ribeirão Preto- USP: CAAE, n° 06825018.2.3001.5440) in tubes

216 containing EDTA (BD Vacutainer CPTTM), according to the manufacturer's
217 instructions. The material was centrifuged at 400 x g for 10 minutes at room
218 temperature. Then, the plasma was discarded and the cell pellet was resuspended in
219 PBS 1X pH 7.4 (GIBCO, BRL). The cells were applied to the Ficoll-Paque™ PLUS
220 gradient column (GE Healthcare Biosciences AB, Uppsala, Sweden). Then, they were
221 centrifuged at 640 x g for 30 minutes at room temperature to obtain the purified
222 mononuclear fraction, which was carefully collected and transferred to a new tube.
223 The cells were washed and the pellet was resuspended in RPMI for the subsequent
224 analysis.

225

226 **Purification of monocytes from healthy donors and differentiation into** 227 **macrophages**

228 The PBMCs were quantified and the monocytes (CD14⁺ cells) were purified using
229 positive selection with magnetic nanoparticles (BD). Briefly, PBMCs were labeled
230 with BD IMag™ Anti-human CD14 Magnetic Particles - DM. The cells were
231 transferred to a 48-well culture plate and placed over a magnetic field of the cell
232 separation. Labeled cells migrated toward the magnet (positive fraction) whereas
233 unlabeled cells were drawn off (negative fraction). The plate was then removed from
234 the magnetic field for resuspension of the positive fraction. The separation was
235 repeated twice to increase the purity of the positive fraction. The CD14⁺ monocytes
236 resulting cells from this process were used for experiments or cultured in RPMI 1640
237 (GIBCO, BRL) containing 10% SFB and 50 ng/mL GM-CSF (R&D Systems) for 7
238 days for differentiation into macrophages.

239

240 **Virus stock production and in vitro infection**

241 The SARS-CoV-2 used was Brazil/SPBR-02/2020 strain, isolated from the first
242 Brazilian case of COVID-19. Viral stock was propagated under BSL3 conditions in
243 Vero E6 cells, cultured in Dulbecco minimal essential medium (DMEM)
244 supplemented with heat-inactivated fetal bovine serum (10%) and
245 antibiotics/antimycotics (Penicillin 10,000 U/mL; Streptomycin 10,000 µg/mL). For
246 preparation of viral stocks, Vero cells were infected in the presence of trypsin-TPCK
247 (1µg/µL) for 48 hours at 37°C in a 5% CO₂ atmosphere. When the virus-induced
248 cytopathic effect, the cells were harvested with cell scrapers, and centrifuged (10.000
249 x G). The supernatant was stored at -80°C, and the virus titration was performed in
250 Vero cells using standard limiting dilution to confirm the 50% tissue culture
251 infectious dose (TCID₅₀).

252 For human cells infections, 2x10⁵ purified human monocytes or monocyte derived
253 macrophages were plated in 48 well plates, and infected with SARS-CoV-2 at
254 Multiplicity of Infection (MOI) of MOI0.2, MOI1, and MOI5. After 2 hours of viral
255 infection, the cells were washed with PBS1x, and a new medium (RPMI 10% FBS
256 without Fenol Red) was added. Cells were incubated for 24h at 37°C in the presence
257 of 5% CO₂ atmosphere. After incubation, cells were processed for
258 immunofluorescence assays and the supernatant was collected for determination of
259 viral loads, cytokine production and LDH quantification.

260

261 **RT-PCR for SARS-CoV-2**

262 Detection of SARS-CoV-2 was performed with primer-probe sets for 2019-nCoV_N2
263 and gene E, according to USA-CDC and Charité group protocols^{12,13}. The genes
264 evaluated (N2, E, and RNase-P housekeeping gene) were tested by one-step real-time
265 RT-PCR using total nucleic acids extracted with Trizol® (Invitrogen, CA, EUA) from

266 50µL of cells supernatants in order to measure the genome viral load from the in vitro
267 assays. All real-time PCR assays were done on Step-One Plus real-time PCR
268 thermocycler (Applied Biosystems, Foster City, CA, USA). Briefly, RNA extraction
269 was performed by Trizol®. A total of 100 ng of RNA was used for genome
270 amplification, adding specific primers (20 µM), and probe (5 µM), and with TaqPath
271 1-Step qRT-PCR Master Mix (Applied Biosystems, Foster City, CA, USA), with the
272 following parameters: 25°C for 2 min, 50°C for 15 min, 95°C for 2 min, followed by
273 45 cycles of 94 °C for 5 s and 60 °C for 30s. Primers used were: N2 fwd: 5'-TTA
274 CAA ACA TTG GCC GCA AA-3'; N2 rev: 5'-GCG CGA CAT TCC GAA GAA-3';
275 N2 probe: 5'-FAM-ACA ATT TGC CCC CAG CGC TTC AG-BHQ1-3'¹³; E fwd:
276 5'-ACA GGT ACG TTA ATA GTT AAT AGC GT-3' ; E rev: 5'-ATA TTG CAG
277 CAG TAC GCA CAC A-3' ; E probe: 5'-AM-ACA CTA GCC ATC CTT ACT GCG
278 CTT CG-BHQ-1-3'¹²; RNase-P fwd: 5'-AGA TTT GGA CCT GCG AGC G-3';
279 RNase-P rev: 5'-GAG CGG CTG TCT CCA CAA GT-3'; RNase-P probe: 5'-FAM-
280 TTC TGA CCT GAA GGC TCT GCG CG - BHQ-1-3'¹³.

281

282 **Evaluation of active caspase-1 activity and LDH release in cultured cells**

283 For LDH determination, 2 x 10⁵ human CD14⁺ cells or human monocyte derived-
284 macrophages were plated on 48-well plates in RPMI 10% FBS and incubated
285 overnight. In the following day, cells were infected with SARS-CoV-2 using MOI
286 0.2, MOI 1, and MOI 5 in RPMI without Phenol Red (3.5 g/L HEPES, 2 g/L
287 NaHCO₃, 10.4 g/L RPMI without Phenol Red, 1% glutamine, pH 7.2) and incubated
288 for 24 h. The supernatant was collected and LDH release was measured using
289 CytoTox 96® Non-Radioactive Cytotoxicity Assay (Promega, Winsconsin, USA)
290 following the manufacturer's instructions. To evaluate caspase-1 activation, 5 x 10⁵

291 PBMC from COVID-19 patients or healthy donors were centrifuged (400g, 10
292 minutes) and cells were labeled for 30 minutes with the FLICA carboxyfluorescein
293 reagent (FAM – YVAD – FMK, Immunochemistry Technologies, LLC), as
294 recommended by the manufacturer. The cells were then washed two times with PBS
295 1x, and fixed with fixative reagent provided by manufacture. Acquisition was
296 performed in fixed cells in flow cytometer (BD Accuri™ C6) and then analyzed using
297 “FlowJo” (Tree Star, Ashland, OR, USA) software. To evaluate caspase-1 activity in
298 supernatants, 2×10^5 PBMCs were plated in 96 wells plate, and incubated overnight.
299 To measure caspase-1 activity, the supernatants were collected, and incubated with
300 the Luciferin WEHD-substrate provided by the Caspase-Glo 1 Assay (Promega).
301 After 1 hour incubation at room temperature, luminescence was measured using
302 SpectraMax i3 system (Molecular Devices).

303

304 **Immunofluorescence staining of isolated cells**

305 For staining PBMCs from COVID-19 patients, a total of 5×10^5 PBMCs were plated in
306 8 wells chamber slides for 1 h in RPMI without FBS for cell adhesion before fixation.
307 For staining cells infected in vitro a total of 2×10^5 human monocytes or monocyte
308 differentiated macrophages were plated in 24-wells plate containing coverslips and
309 infected with SARS-CoV-2 at indicated MOI for 16h. For fixation of the samples,
310 tissue culture supernatants were removed and cells were fixed with 4%
311 paraformaldehyde (PFA) for 20 minutes at room temperature. PFA was removed,
312 cells were washed with PBS1x, and the coverslips or chambers were processed for IF
313 as described. Cells were blocked and permeabilized using PBS 1x with goat serum
314 and 0.05% saponin for 1h at room temperature. Primary antibodies mix of rabbit mAb
315 anti-NLRP3 (Cell Signaling, 1:1000) were diluted in blocking solution and added to

316 each chamber/coverslip. After 1h of incubation the samples were washed with PBS 1x
317 and secondary antibodies were added and incubated for 1h at room temperature.
318 Secondary antibodies used were goat anti-rabbit 488 (Invitrogen,1:3000) and goat
319 anti-rabbit 594 (Life Technologies,1:3000). Slides were washed and mounted using
320 DAPI (1mM) and ProLong (Invitrogen).

321

322 **Lung samples from autopsies and immunofluorescence and imaging**

323 Adapted minimally invasive autopsies were performed in COVID-19 patients ¹⁵⁻¹⁷.
324 Briefly, a mini thoracotomy (3cm) was done under the main area of lung injury
325 identified by prior x-ray or computed tomography. The lung parenchyma is clamped
326 by Collins Forceps, cut and fixed in 10% buffered formalin. Pulmonary tissue
327 samples were stained with hematoxylin and eosin (H&E) and immunostaining as
328 reported ^{18 19}. The slides were incubated with the primary antibodies, rabbit anti-
329 CD14 mAb (Abcam, 1:200) and mouse anti-Nlrp3 mAb (AdipoGen, 1:200), for 2h at
330 room temperature or overnight at 4°C. Goat anti-mouse Alexa fluor-647 (Invitrogen)
331 or goat anti-rabbit Alexa fluor-594 (Invitrogen) were used as secondary antibodies.
332 Images were acquired by Axio Observer combined with LSM 780 confocal device
333 with 630 x magnification (Carl Zeiss). Minimally invasive autopsies were approved
334 by the FMRP/USP Ethical Committee (protocol #4.089.567).

335

336 **Sequential immunoperoxidase labeling and erasing**

337 Tissue sections from paraffin-embedded lung fragments obtained from COVID-19
338 fatal cases were tested by immunohistochemistry (IHC) using anti-SARS-CoV-2
339 polyclonal antibody for in situ detection of SARS-CoV-2. Sequential
340 immunoperoxidase labeling and erasing (SIMPLE) was then performed to determine

341 additional markers after SARS-CoV-2 immune stain, using antibodies to CD14
342 (Abcam, 1:100 dilution), NLRP3 (Cell Signaling, 1:100 dilution) (Glass et al., 2009).
343 After the incubation with primary antibody, the slides were incubated with immune-
344 peroxidase polymer anti-mouse visualization system (SPD-125, Spring Bioscience,
345 Biogen) and then with the chromogen substrate AEC peroxidase system kit (SK-4200,
346 Vector Laboratories, Burlingame, CA). Microphotographs after immunostaining of
347 tissue slides were scanned on a VS120 Olympus. After high-resolution scanning,
348 slides coverslips were removed in PBS and dehydrated through ethanol gradient to
349 95% ethanol. Slides were incubated in ethanol series until erasing AEC color reaction.
350 Following rehydration, antibodies were eluted by incubating sections in 0.15 mM
351 $\text{KMnO}_4/0.01 \text{ M H}_2\text{SO}_4$ solution for 2 min, followed immediately by a distilled water
352 wash. Tissue was then restained as indicated in the blocking step.

353

354 **Cytokine quantification in sera**

355 Active caspase-1 (Casp1p20) and IL-18 levels were evaluated by ELISA assay (R&D
356 Systems) in the serum from patients with COVID-19 or health donors following
357 manufacturer's instructions. TNF- α , IL-2, IL-4, IL-6, IL-10, IFN- γ , and IL-17 were
358 quantified in the serum from patients with COVID-19 or health donors using a human
359 CBA cytokine kit (Th1/Th2/Th17 Cytokine Kit, BD Biosciences) following
360 manufacturer's instructions. IL-1 β in the tissue culture supernatants of human
361 monocytes or macrophages cells infected with SARS-CoV-2 was quantified by
362 ELISA (R&D Systems) following manufacturer's instructions.

363

364 **Statistics**

365 Statistical significance for the linear analysis was determined by either two-tailed
366 paired or unpaired Student t-test for data that reached normal distribution and Mann-
367 Whitney was used for not normally distributed data. These statistical procedures and
368 graph plots were performed with GraphPad Prism 8.4.2 software. In addition,
369 longitudinal analyses were implemented to describe variation in IL-18 and Casp1p20
370 production along time, considering patients' outcomes and sex as fixed factors. These
371 analyses were performed in R (version 4.0.2) using RStudio (version 1.3.1056), and
372 are detailed as R Markdown object at the supplementary material. The patients'
373 outcomes were divided into 3 categories (37 patients in total, 16 women and 21 men):
374 death (n = 10 individuals, a total of 25 samples), mild recovery (patients that were
375 hospitalized but did not require mechanical ventilation; n = 17 individuals, a total of
376 53 samples) and critical recovery (patients that required mechanical ventilation at the
377 UCI and recovered; n = 10 individuals, a total of 27 samples). Activation of IL-18 and
378 Casp1 were evaluated separately using full models that considered the interaction of
379 time ('Day.sampled') with patients' outcomes ('Outcome') or sex ('Sex') and
380 included individuals ('Patient.ID') as a random factor to control for repeated
381 measures and individual effects. Normality and homoscedasticity of the dataset were
382 verified and refuted for time series dataset (see RMarkdown object), and analyses
383 were implemented using the glmmTMB package²⁰ in a generalized mixed model's
384 (GMM's) approach with 'gamma' distribution and 'log' link function. Akaike
385 information criterion for finite samples (AICc) was used to select the best models
386 from the full ones using MuMIn²¹. Models having AICc values within 2 units of the
387 best-fit model were considered to have substantial support²²; adequate residuals
388 distributions were confirmed and representative graphics and tables were constructed

389 using the packages DHARMA²³, ggeffects²⁴ and broom.mixed²⁵ - see RMarkdown
390 object to access all parameterization in **Supplemental data**.

391

392 **Study approval**

393 The procedures followed in the study were approved by the National Ethics
394 Committee, Brazil (CONEP, CAAE: 30248420.9.0000.5440). Written informed
395 consent was obtained from recruited patients.

396

397 **Acknowledgments**

398 We are grateful to Maira Nakamura, Bárbara Moreira de Carvalho e Silva and Laura
399 Khouri for technical assistance.

400

401 **Author Contributions**

402 T.S.R., and D.S.Z. conceived the study. T.S.R., K.S.G.S. A.Y. I., A.B., S.O., L.A.,
403 A.V.G., D.B.P., W.A.A. designed the experiments, defined parameters, collected and
404 processed PBMC and sera samples and analyzed data. R.C., J.E.T., D.C.N., M.H.F.L.,
405 C.M.S.S., D.B.C. processed PBMC samples. L.D.C. supervised the collection of
406 PBMC samples from patients. T.S.R., R.B.M., I.A.C., M.C.P. performed the
407 experiments with viral infections. A.T.F., S.S.B., L.S., M.N.B. performed minimally
408 invasive autopsy. K.S.G.S., F.P.V. stained and analyzed autopsy tissues. A.Y.I,
409 F.C.B., T.K. performed bioinformatic analyses, designed and conducted statistical
410 analyses of the data. N.B.A., M.C.G., L.P.B., M.I.F.L., M.N.B., R.C.S., F.C.V., M.A.,
411 R.L., S.C.L.A., F.R.O., R.D.R.O., P.L assisted in patient recruitment, collected patient
412 specimens and the epidemiological and clinical data. P.L. supervised and R.D.R.O.
413 helped clinical data management. T. M.C, J.C.A., F.Q.C., L.D.C., F.G.F., T.K.,

414 A.T.F., E.A., R.D.R.O., P.L., helped with interpretations of the data. T.S.R., and
415 D.S.Z. drafted the manuscript. All authors helped editing the manuscript. D.S.Z.
416 secured funds and supervised the project.

417

418

419 **Competing interests**

420 The authors declare no competing financial interests.

421

422 **Materials & Correspondence**

423 dszamboni@fmrp.usp.br

424

425 **Funding**

426 FAPESP grants (2013/08216-2, 2019/11342-6 and 2020/04964-8), CNPq and CAPES
427 grants.

428

429

430 **References**

431

- 432 1 Merad, M. & Martin, J. C. Author Correction: Pathological inflammation in
433 patients with COVID-19: a key role for monocytes and macrophages. *Nature*
434 *reviews. Immunology* **20**, 448, doi:10.1038/s41577-020-0353-y (2020).
- 435 2 Chen, G. *et al.* Clinical and immunological features of severe and moderate
436 coronavirus disease 2019. *The Journal of clinical investigation* **130**, 2620-
437 2629, doi:10.1172/JCI137244 (2020).
- 438 3 Han, Y. *et al.* Lactate dehydrogenase, an independent risk factor of severe
439 COVID-19 patients: a retrospective and observational study. *Aging* **12**, 11245-
440 11258, doi:10.18632/aging.103372 (2020).
- 441 4 Huang, C. *et al.* Clinical features of patients infected with 2019 novel
442 coronavirus in Wuhan, China. *Lancet* **395**, 497-506, doi:10.1016/S0140-
443 6736(20)30183-5 (2020).
- 444 5 Lucas, C. *et al.* Longitudinal analyses reveal immunological misfiring in
445 severe COVID-19. *Nature*, doi:<https://doi.org/10.1038/s41586-020-2588-y>
446 (2020).

- 447 6 Broz, P. & Dixit, V. M. Inflammasomes: mechanism of assembly, regulation
448 and signalling. *Nature reviews. Immunology* **16**, 407-420,
449 doi:10.1038/nri.2016.58 (2016).
- 450 7 Hauenstein, A. V., Zhang, L. & Wu, H. The hierarchical structural architecture
451 of inflammasomes, supramolecular inflammatory machines. *Current opinion*
452 *in structural biology* **31**, 75-83, doi:10.1016/j.sbi.2015.03.014 (2015).
- 453 8 Alfaidi, M. *et al.* Neutrophil elastase promotes interleukin-1beta secretion
454 from human coronary endothelium. *The Journal of biological chemistry* **290**,
455 24067-24078, doi:10.1074/jbc.M115.659029 (2015).
- 456 9 Guma, M. *et al.* Caspase 1-independent activation of interleukin-1beta in
457 neutrophil-predominant inflammation. *Arthritis and rheumatism* **60**, 3642-
458 3650, doi:10.1002/art.24959 (2009).
- 459 10 Joosten, L. A. *et al.* Inflammatory arthritis in caspase 1 gene-deficient mice:
460 contribution of proteinase 3 to caspase 1-independent production of bioactive
461 interleukin-1beta. *Arthritis and rheumatism* **60**, 3651-3662,
462 doi:10.1002/art.25006 (2009).
- 463 11 Zamboni, D. S. *et al.* The Birc1e cytosolic pattern-recognition receptor
464 contributes to the detection and control of Legionella pneumophila infection.
465 *Nature immunology* **7**, 318-325, doi:10.1038/ni1305 (2006).
- 466 12 Corman, V. M. *et al.* Detection of 2019 novel coronavirus (2019-nCoV) by
467 real-time RT-PCR. *Euro surveillance : bulletin European sur les maladies*
468 *transmissibles = European communicable disease bulletin* **25**,
469 doi:10.2807/1560-7917.ES.2020.25.3.2000045 (2020).
- 470 13 Nalla, A. K. *et al.* Comparative Performance of SARS-CoV-2 Detection
471 Assays Using Seven Different Primer-Probe Sets and One Assay Kit. *Journal*
472 *of clinical microbiology* **58**, doi:10.1128/JCM.00557-20 (2020).
- 473 14 Wu, Z. & McGoogan, J. M. Characteristics of and Important Lessons From
474 the Coronavirus Disease 2019 (COVID-19) Outbreak in China: Summary of a
475 Report of 72314 Cases From the Chinese Center for Disease Control and
476 Prevention. *Jama*, doi:10.1001/jama.2020.2648 (2020).
- 477 15 Avrahami, R., Watemberg, S., Hiss, Y. & Deutsch, A. A. Laparoscopic vs
478 conventional autopsy. A promising perspective. *Archives of surgery* **130**, 407-
479 409, doi:10.1001/archsurg.1995.01430040069014 (1995).
- 480 16 Damore, L. J., 2nd, Barth, R. F., Morrison, C. D., Frankel, W. L. & Melvin,
481 W. S. Laparoscopic postmortem examination: a minimally invasive approach
482 to the autopsy. *Annals of diagnostic pathology* **4**, 95-98, doi:10.1016/s1092-
483 9134(00)90018-2 (2000).
- 484 17 Vejrosta, Z. & Bilder, J. [Pathogenesis of excessive mobility of the
485 temporomandibular joint]. *Ceskoslovenska stomatologie* **75**, 119-124 (1975).
- 486 18 Fabro, A. T. *et al.* The Th17 pathway in the peripheral lung microenvironment
487 interacts with expression of collagen V in the late state of experimental
488 pulmonary fibrosis. *Immunobiology* **220**, 124-135,
489 doi:10.1016/j.imbio.2014.08.011 (2015).
- 490 19 Fabro, A. T. *et al.* Yellow Fever-induced Acute Lung Injury. *American*
491 *journal of respiratory and critical care medicine* **200**, 250-252,
492 doi:10.1164/rccm.201711-2267IM (2019).
- 493 20 Brooks, M. E. *et al.* glmmTMB Balances Speed and Flexibility Among
494 Packages for Zero-inflated Generalized Linear Mixed Modeling. *The R*
495 *Journal* **9**, 378-400 (2017).

496 21 Barton, K. MuMIn: Multi-Model Inference. R package version 1.43.17.
497 <https://CRAN.R-project.org/package=MuMIn> (2020).
498 22 Burnham, K. P. & Anderson, D. R. Model Selection and Multimodel
499 Inference: a practical information-theoretic approach (2002).
500 23 Hartig, F. DHARMA: Residual Diagnostics for Hierarchical (Multi-Level /
501 Mixed) Regression Models. R package version 0.3.2.0. [https://CRAN.R-](https://CRAN.R-project.org/package=DHARMA)
502 [project.org/package=DHARMA](https://CRAN.R-project.org/package=DHARMA) (2020).
503 24 Lüdtke, D.ggeffects: Tidy Data Frames of Marginal Effects from Regression
504 Models. *Journal of Open Source Software* **3**, 772, doi:10.21105/joss.00772
505 (2018).
506 25 Bolker, B. & Robinson, D. broom.mixed: Tidying Methods for Mixed Models.
507 R package version 0.2.6. <https://CRAN.R-project.org/package=broom.mixed>
508 (2020).
509
510
511

512

513 **Figure Legends**

514

515 **Figure 1. Infection of primary human monocytes with SARS-CoV-2 triggers**

516 **inflammasome activation. (A-E)** Human CD14⁺ monocytes were primed or not with

517 PAM3Cys (300ng/mL) for 4 hours and infected with SARS-CoV-2 at a multiplicity

518 of infection (MOI) of 0.2, 1 and 5 for 24 h. Mock was used as a negative infection

519 control, and nigericin as a positive NLRP3 activation control. (A) LDH release was

520 measured in the supernatants from 5 different donors. Triton (9%) was used to induce

521 cell death and estimate 100% death. (B) the percentage of cell containing NLRP3

522 puncta was estimated in cells from 5 different donors. (C) A representative image of a

523 monocyte containing NLRP3 puncta (green, indicated by arrows) and replicating

524 SARS-CoV-2, depicted by anti-dsRNA antibody staining (red, indicated by an

525 arrowhead) is shown. Nuclei stained in blue. Scale bar 5 μ m. (D) IL-1 β production

526 was analyzed in the tissue culture supernatants of monocytes infected or not infected

527 (MOCK) with the indicated MOI in experimental replicates. (E) Viral loads in the

528 cell culture supernatants were estimated by RT-PCR in monocytes infected for 8 and

529 24 hs at the indicated MOI. (F) Monocytes from one donor were derived into

530 macrophage and primed with PAM3Cys (300ng/mL) for 4 hours and infected with

531 SARS-CoV-2 at a MOI of 1, 5 and 10 and 20 for 24 h. LDH were measured in the

532 supernatants of experimental replicates. Mock and UV-irradiated virus (U.V. Inat.)

533 was used as a negative infection control, and nigericin as a positive control. * $P <$

534 0.05, as determined by Student's t-test. Box shows the average \pm SD of the values.

535

536 **Figure 2. Inflammasome activation in COVID-19 patients. (A-C)** Cytokine
537 concentration in the serum control individuals (CT, n=42 to ELISA and 45 to CBA)
538 and COVID-19 patients (COVID-19 P, n=124 to ELISA and 92 to CBA; all tested
539 positive using RT-PCR). Active caspase-1 (Casp1p20, A) and IL-18 (B) were
540 measured by ELISA, and IL-6 (C) were measured by CBA. Data are shown as Log10-
541 transformed concentrations in pg/mL. (D-I) Peripheral Blood Mononuclear Cells
542 (PBMCs) were isolated from fresh blood of CT or COVID-19 P. (D-E) FAM-YVAD
543 positive PBMCs were estimated by FACS using FLICA Caspase-1 Assay Kit. (D)
544 Representative histograms of one representative CT and one COVID-19 P indicate the
545 gate for determination of the percentage of FAM-YVAD⁺ cells. (E) The percentage
546 of FAM-YVAD⁺ cells for the 32 CT and 47 COVID-19 P. (F) PBMCs from COVID-
547 19 P were stained with anti-dsRNA (red, indicating SARS-CoV-2 replication) and
548 anti-NLRP3 (green) for determination of NLRP3 puncta (indicated by white arrows).
549 Dapi (blue) stains the nuclei. Scale bar 20 μ m. (G) The percentage of cells with
550 NLRP3 puncta are shown for 24 CT and 17 COVID-19 P. (H) PBMCs from 18 CT
551 and 46 COVID-19 P were maintained in culture for 16 hours and the supernatants
552 were assayed for caspase-1 activity using the Caspase-Glo 1 Assay (H). (I) PBMCs
553 from 6 CT or 18 COVID-19 P were maintained in culture for 16 hours and IL-1 β
554 production were estimated by ELISA. * $P < 0.05$, ** $P < 0.01$ and *** $P < 0.001$ as
555 determined by Student's t-test or Mann Whitney. Each dot represents the value from a
556 single individual. Box shows average \pm SD of the values.
557

558 **Figure 3. Lung histopathological analysis and NLRP3 activation in fatal cases of**
559 **COVID-19.** Representative pulmonary histological findings in COVID-19 patient
560 (COVID-19 P), autopsied by ultrasound guided-minimally invasive autopsy. (A, B)
561 Representative Immunohistochemical image of tissues from Control (CT, A) or
562 COVID-19 P (B) stained with anti-SARS-CoV-2. Scale bar 50 μm . (C-D) Multiplex
563 staining by sequential immunohistochemistry staining with anti-SARS-CoV-2, anti-
564 CD14 and anti-NLRP3 arrows indicates infected CD14+ cells expressing NLRP3 .
565 Scale bar 20 μm (C) and 10 μm (D). (E) Quantification of NLRP3 puncta in
566 pulmonary tissues of 5 CT and 6 COVID-19 P. (F, I) Multiphoton microscopy of
567 tissues stained with anti-NLRP3 antibody indicates NLRP3 puncta (red, indicated by
568 black arrows) in the pulmonary tissues. DAPI stains nuclei (blue). (I) NLRP3 puncta
569 in a cell inside a venule (dotted white line). Scale bar 10 μm .

570

571

572 **Figure 4. Inflammasome activation influences the clinical outcome of COVID-19.**

573 (A) Correlation matrix of Casp1p20 and IL-18 levels in the serum of COVID-19
574 patients at the hospitalization day with patient characteristics and clinical parameters.
575 (B-J) Correlations of Casp1p20 with IL-18 (B), Casp1p20 with IL-6 (C), Casp1p20
576 with lactate dehydrogenase (LDH) (D), Casp1p20 with C-reactive protein (CRP), IL-
577 18 with IL-6 (F) and IL-18 with CRP (G). (H,I) Levels of Casp1p20 (H) and IL-18 (I)
578 in patients that required (MV+, blue box) or not (MV-, red box) mechanical
579 ventilation. (J,K) Levels of Casp1p20 (J) and IL-18 (K) in patients with
580 Mild/Moderate (yellow box) or Severe COVID-19 (pink box). (L,M) Levels of
581 Casp1p20 (L) and IL-18 (M) in survivors (green box) or non-survivors (purple box).
582 The levels of Casp1p20 and IL-18 were measured by ELISA and are shown as
583 Log₁₀-transformed concentrations in pg/mL. * $P < 0.05$, ** $P < 0.01$ and *** $P <$

584 0.001 as determined by Student's t-test. Each dot represents value to form a single
585 individual. Box shows average \pm SD of the values. (N, O) Derived predictions from
586 the best-fit models retained in Casp1p20 (N) and IL-18 (O) longitudinal analyses; IL-
587 18 Model (O) comprises variation in the intercept among patients' groups: Death
588 (Red), Critical/Recovery (orange) and Mild/Recovery (blue).

589

590

591 **Fig. S1. Cytokine production in COVID-19 patients.** Cytokine concentration in the
592 serum control individuals (CT, n=45) and COVID-19 patients (COVID-19 P, n=92;
593 all tested positive using RT-PCR). IL-10 (A), IL-4 (B), IFN- γ (C), TNF- α (D) and IL-
594 17A (E) were measured by CBA. Data are shown as Log10-transformed
595 concentrations in pg/mL. ** $P < 0.01$ and *** $P < 0.001$ as determined by Student's t
596 test. Each dot represents the value form a single individual. Box show average \pm SD
597 of the values.

598

599 **Fig. S2. Association of inflammasome activation with clinical characteristics and**
600 **comorbidities.** (A) Matrix correlation of Casp1p20 and IL-18 levels in the serum of
601 COVID-19 patients at the hospitalization day with clinical parameters and
602 comorbidities. (B-S) Levels of Casp1p20 (B, D, F, H, J, L, N, P, R) and IL-18 (C, E,
603 G, I, K, M, O, Q, S) in patients with clinical parameters such as cultivable bacteria in
604 the blood (B, C), nephropathy (D, E), obesity (F, G), gender (H, I), cerebrovascular
605 accident (J, K), pneumopathy (L, M), immunodeficiency (N, O) and neoplasia (P, Q)
606 and smoking (R, S). The levels of Casp1p20 and IL-18 were measured by ELISA and
607 are shown as Log10-transformed concentrations in pg/mL. ** $P < 0.01$ as determined

608 by Student's t test. Each dot represents value form a single individual. Box show

609 average \pm SD of the values.

610

611 **Table S1 – Demographic and clinical characteristics of COVID-19**

612 **patients.**

613

614

615

616

617 **Table S1: COVID-19 patient characteristics**

Demographics		%
Number	124	
Age (years)	59.25±18.01	
Female	50	40%
Comorbidities		
Hypertension	61	49%
Obesity	61	49%
Diabetes	46	37%
History of smoking	33	26%
Heart disease	23	18%
Lung disease	20	16%
Kidney disease	13	10%
Cancer	11	8%
History of stroke	9	7%
Immunodeficiency	6	4%
Autoimmune diseases	2	1%
Laboratorial findings		
CRP (mg/dL)*	12.55±8.95	
D-Dimers (µg/mL)**	2.47±2.59	
LDH (U/L)#	565.147±325.9	
Ferritin (ng/mL)&	1225.07±1762.9	
Haemoglobin (g/dL)	12.31±2.34	
Neutrophils (cell/mm ³)	6728.443±3903.57	
Lymphocytes (cell/mm ³)	1307.37±789.1	
Platelets (count/mm ³)	253426.2±111616.3	
Medications		
Heparin	112	90%
Antibiotics	110	88%
Glucocorticoids	58	46%
Oseltamivir	56	45%
Antimalarial	45	36%
Respiratory status		
Mechanical ventilation	56	45%
Nasal-cannula oxygen	111	89%
pO ₂	77.77±29.17	
SatO ₂	93.37±5.72	
Disease Severity		
Mild	7	6%
Moderate	49	39%
Severe	68	55%
Outcome		
Deaths	34	27%

618

619

620

*CRP: C-reactive protein (Normal value <0.5 mg/dL); **D-dimers (NV <0.5 µg/mL); #LDH: lactate dehydrogenase (Normal range: 120-246 U/L); &Ferritin (NR: 10-291 ng/mL)

Figure 1. Rodrigues et al.

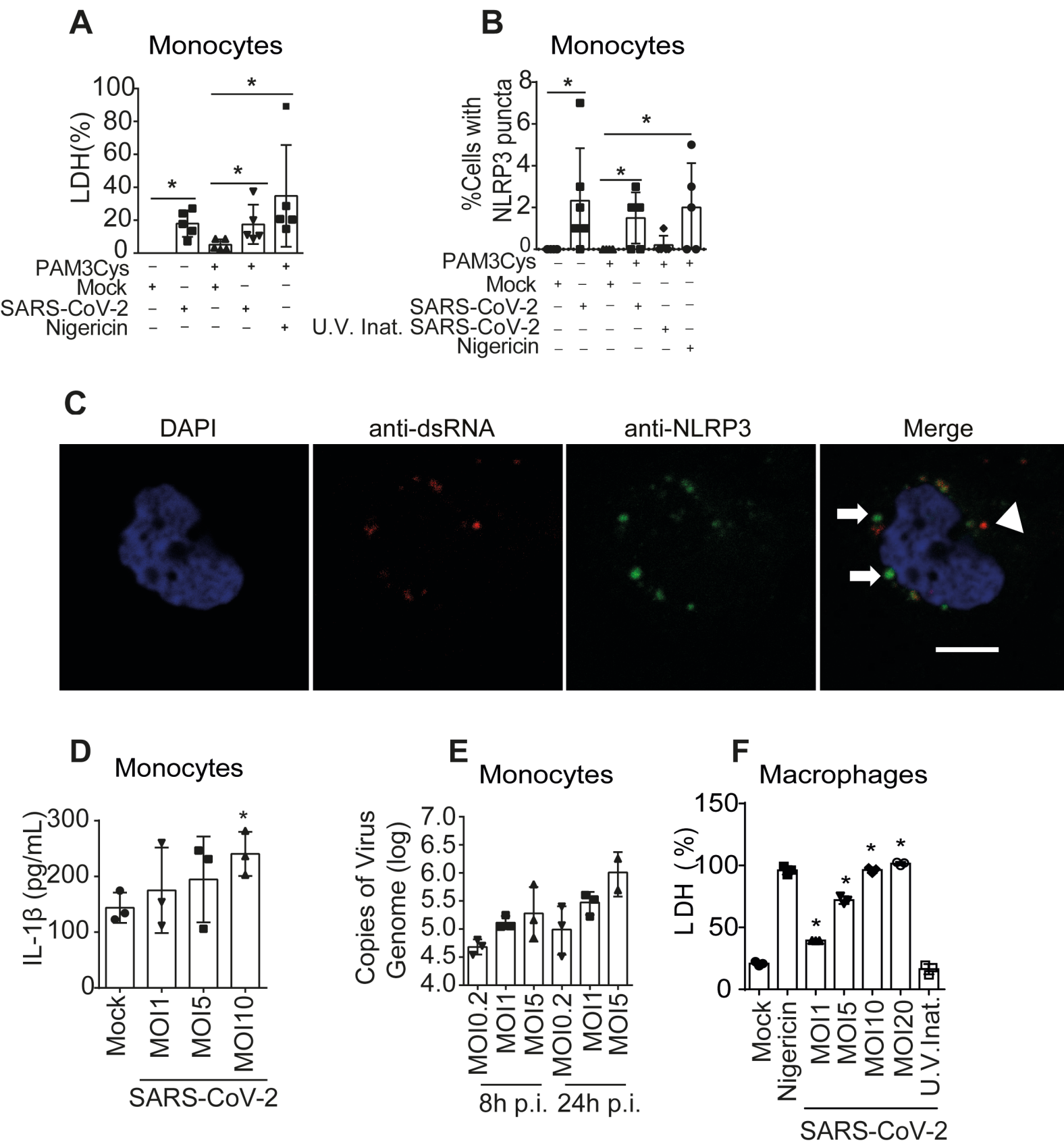
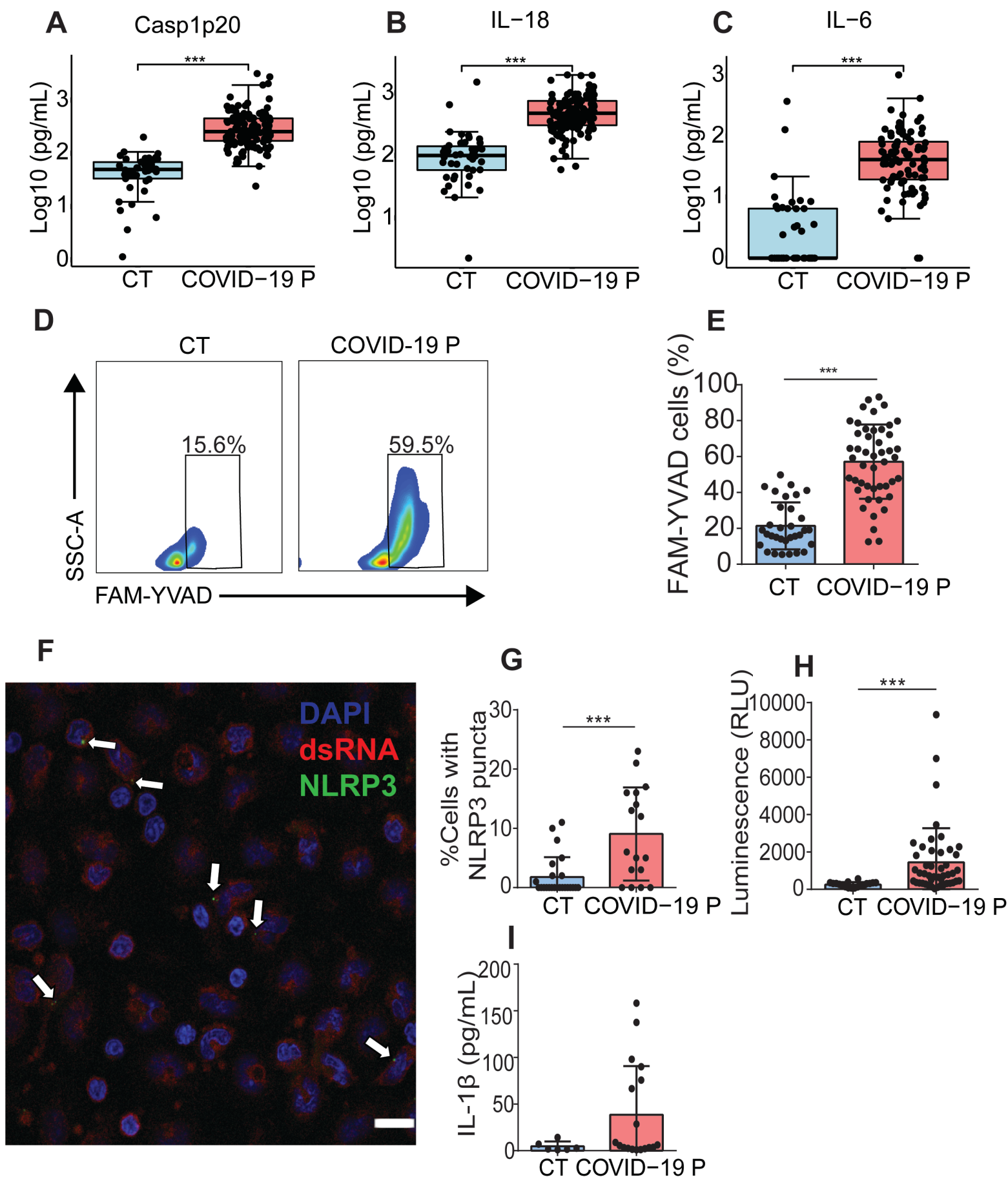


Figure 2. Rodrigues et al.



anti-SARS-CoV-2 COVID-19 P

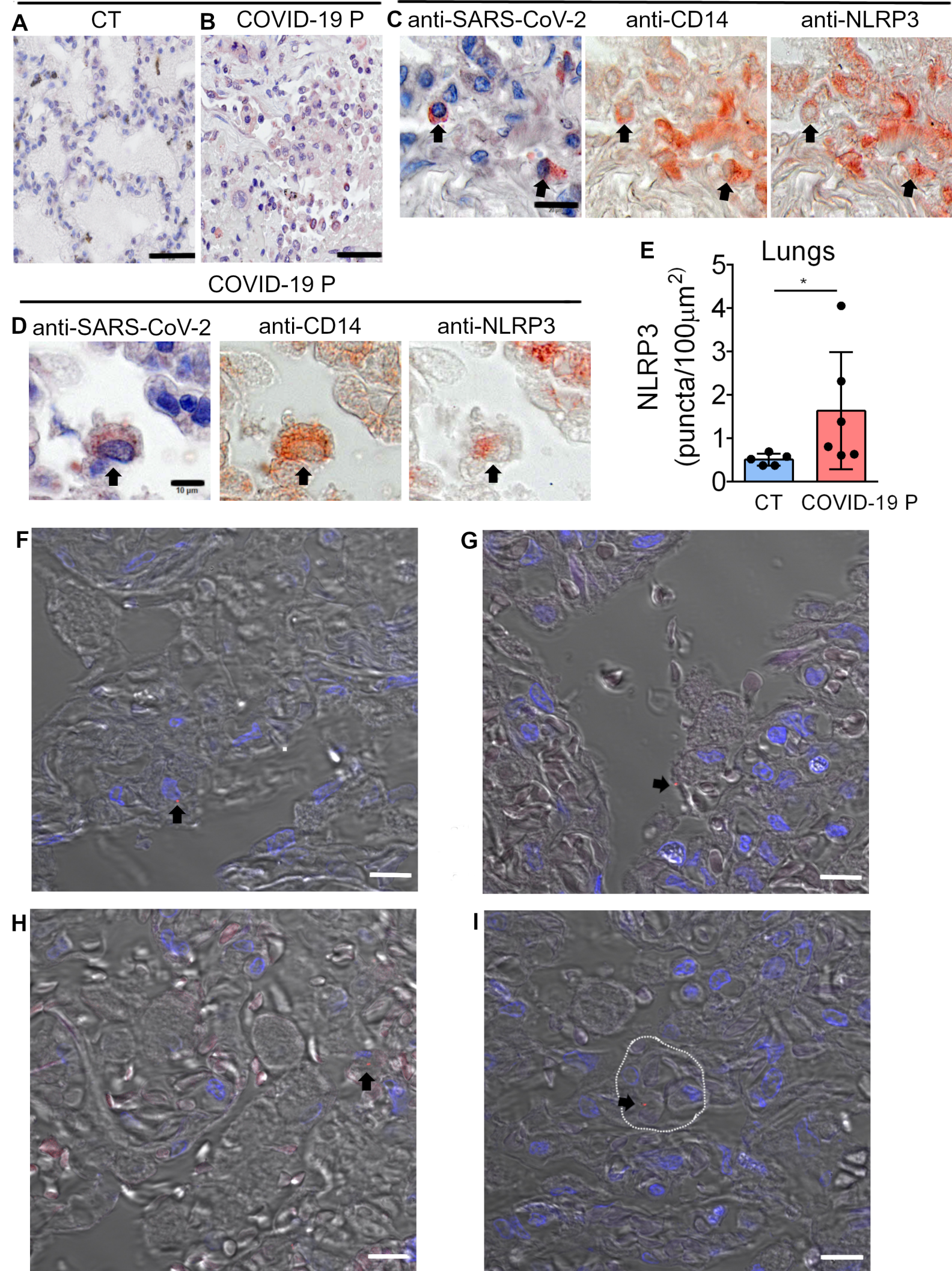


Figure 4. Rodrigues et al.

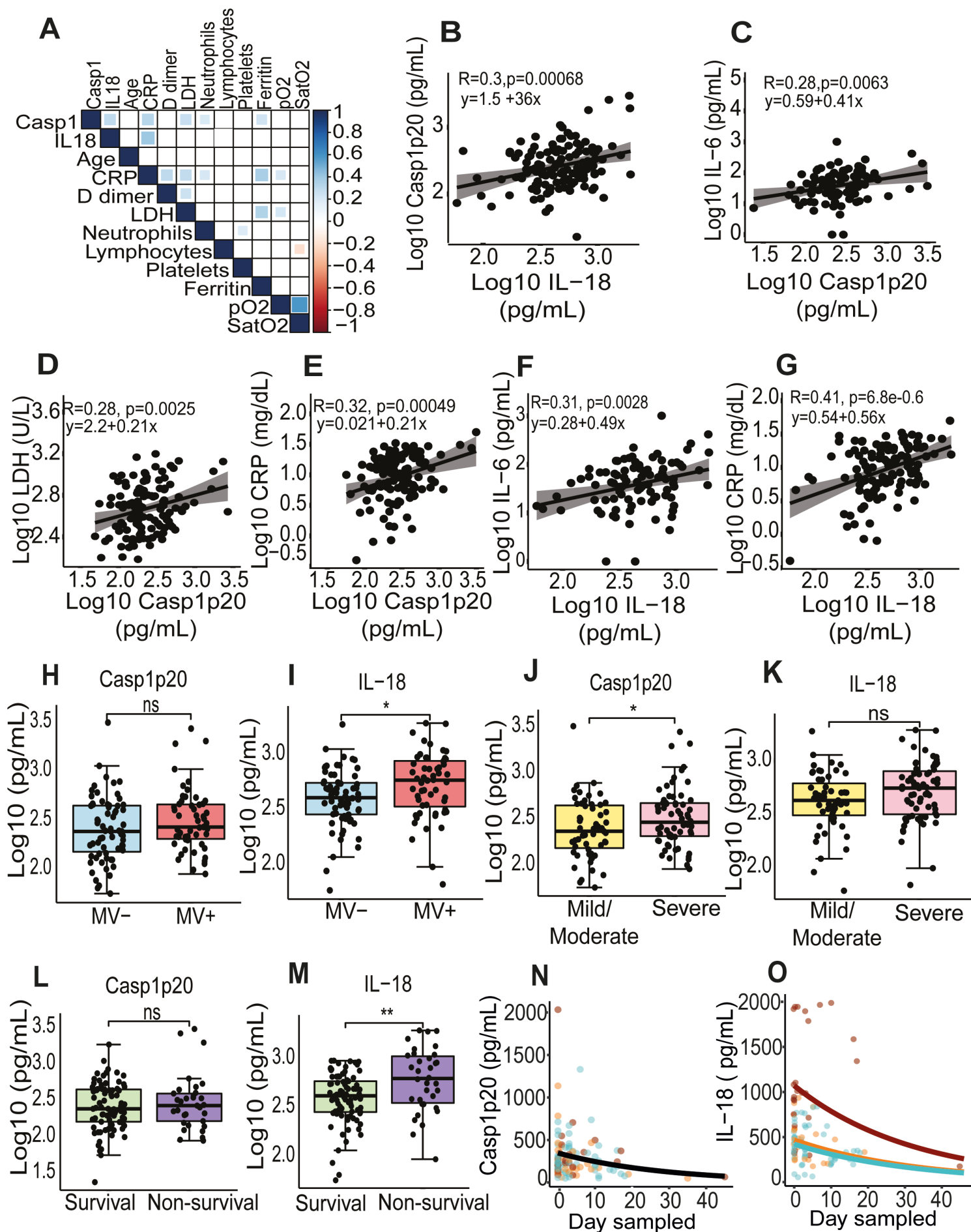


Fig. S1. Rodrigues et al.

